

LEIBNIZ INSTITUTE FOR TROPOSPHERIC
RESEARCH

BACHELOR THESIS

BACHELOR OF SCIENCE METEOROLOGY

Comparison of radiosonde data
from Leipzig to meteorological
profiles of two atmospheric models

author

FINJA BAUMER

first assessor

PROF. DR. ANDREAS MACKE

second assessor

DR. PATRIC SEIFERT

supervisor

DR. HOLGER BAARS

11.10.2022

Contents

1	Introduction	2
2	Data Description and Methods	3
2.1	Radiosonde	3
2.2	GDAS	3
2.3	ECMWF	4
2.4	Variables	4
2.5	Statistical Parameters	5
3	Results	8
3.1	Pressure	8
3.2	Temperature	11
3.3	Wind Velocity	15
3.3.1	Zonal Component u	15
3.3.2	Meridional Component v	17
3.3.3	Absolute Wind Velocity U	18
3.4	Wind Direction	19
3.5	Wind Case Examples	20
3.6	Relative Humidity	24
4	Summary	29
5	Appendix	31

Chapter 1

Introduction

In weather observation and forecasting not only the conditions at ground level are of interest but also the vertical profile of the state of the atmosphere. There are a lot of different options to measure this profile including satellites, RADARs, LIDARs and of course radiosondes. The latter option is the topic of this thesis. They measure pressure, temperature, relative humidity as well as wind velocity and direction in high resolution and accuracy.

The Leibniz Institute for Tropospheric Research (TROPOS) in Leipzig has started doing weekly radiosonde releases since May 2019. The collected data is being compared to model simulations by the European Centre for Medium Range Weather Forecasts (ECMWF) and the Global Data Assimilation System (GDAS) by the National Centers for Environmental Prediction (NCEP). Evaluating the difference between the modelled profile and the real atmospheric stratification will be interesting, in particular with regard to the models different vertical resolutions. Models like this generally use global measurement data for assimilation, including radiosonde measurements. The data of TROPOS is not used in either model which makes it an independent data set for validation.

Chapter 2

Data Description and Methods

2.1 Radiosonde

Radiosondes are an in-situ method for measuring the vertical state of the atmosphere. They combine multiple sensors to detect temperature, relative humidity, pressure and wind (speed and direction). The sensors are contained in a white box made out of polystyrene to minimize errors due to solar radiation and weight respectively. The box is connected to a balloon filled with enough helium to ensure an ascend speed of about $3\text{-}4\text{ m s}^{-1}$. The radiosonde model used at TROPOS is RS41-SGP by Vaisala. It gives high resolution measurements every second with good accuracy. The uncertainties of the variables measured are listed in the table below (also see Vaisala data sheet in appendix):

Table 2.1: Uncertainties of different sensors of the radiosonde RS41-SGP by Vaisala,

variable	uncertainty
temperature	$\left\{ \begin{array}{l} h < 16 \text{ km: } 0.3 \text{ }^\circ\text{C} \\ h > 16 \text{ km: } 0.4 \text{ }^\circ\text{C} \end{array} \right.$
rel. humidity	4 %
pressure	$\left\{ \begin{array}{l} p > 100 \text{ hPa: } 1 \text{ hPa} \\ 3 < p \leq 100 \text{ hPa: } 0.6 \text{ hPa} \end{array} \right.$
wind speed	0.15 m s^{-1}
wind direction	2°

The data considered in this thesis consist of vertical profiles from 120 days between the 24. May 2019 and 12. August 2022. For reference, the radiosondes are released at TROPOS with the coordinates 51.35°N , 12.43°E .

2.2 GDAS

The Global Data Assimilation System (GDAS) is used by the Global Forecast System (GFS), an American model by NCEP. GDAS is a tool created in order to

initialize weather forecasts with observational data by interpolating between observation systems and instruments onto a three dimensional grid (NOAA, 2022). The grid point used is located at 51.0°N, 12.40°E with a 1x1° horizontal resolution in this case. The prediction time is 15 UTC - one hour before the radiosonde is released. Each profile is divided into 23 pre-set pressure levels starting at 1000 hPa using 25 hPa steps until 900 hPa. Above that, it changes to 50 hPa steps. The top level is at 20 hPa. Relative humidity (RH) is calculated with respect to water for $T \geq 0^\circ\text{C}$ and with respect to ice for $T < -20^\circ\text{C}$. A blend of both is used between those boundaries (NOAA, 2021). There is no relative humidity computed for the top two levels (50 and 20 hPa).

2.3 ECMWF

The data used by ECMWF is produced by the Integrated Forecast System (IFS) which also includes observation processing and data assimilation. There are a number of different forecasts available from medium-range to seasonal predictions. Deterministic and ensemble forecasts are also provided. The simulations used for this thesis are from high resolution deterministic medium-range forecasts (HRES) with a temporal resolution of one hour (Tuononen et al., 2019). Here, the 16 UTC profiles are used because that is the approximate time of release of the radiosondes. The horizontal resolution is 9 km ($0.1 \times 0.1^\circ$) with 137 vertical levels. To match the range of the radiosondes of about 25 km altitude, only the first 100 levels are used. The vertical grid spacing is not consistent and varies between 20 and 300 m with higher resolution towards the ground (Tuononen et al., 2019). ECMWF's nearest grid point to Leipzig lies at 51.35°N, 12.51°E.

2.4 Variables

All variables are considered with respect to altitude above mean sea level (MSL). Radiosonde and GDAS already supply the height in this unit while ECMWF gives altitude above ground (tab. 2.2). This needs to be adapted. The ECMWF data sets include a variable called "sfc_height_amsl" which contains the surface height above MSL considered by the model. For the considered grid point the value is 135.9 m so this amount has been added to each profile.

As can be seen in Table 2.2, the models compute the zonal and meridional wind components u and v while the radiosondes measure wind direction α and advection speed U . The horizontal wind components can be converted into direction and speed using the following equations:

$$U = \sqrt{u^2 + v^2} \quad (2.1)$$

$$\alpha = \arctan2(u, v) \cdot \frac{180^\circ}{\pi} + 180 \quad (2.2)$$

Conversely, direction and speed can be converted into the horizontal wind components:

$$u = -U \cdot \sin\left(\alpha \cdot \frac{\pi}{180}\right) \quad (2.3)$$

$$v = -U \cdot \cos\left(\alpha \cdot \frac{\pi}{180}\right) \quad (2.4)$$

Table 2.2: Used variables from the data sets, their description/long name and the corresponding unit

variable	long name	unit
radiosonde		
HeightMSL	Height above mean sea level	km
P	pressure	hPa
Temp	temperature	°C
Dir	wind direction	°
Speed	wind speed (absolute)	m s ⁻¹
RH	relative humidity	%
GDAS		
HGTS	height above mean sea level	km
TEMP	temperature	°C
UWIND	zonal wind	m s ⁻¹
VWIND	meridional wind	m s ⁻¹
RELH	relative humidity	%
ECMWF		
height	height above ground	km
pressure	pressure	hPa
temperature	temperature	°C
uwind	zonal wind	m s ⁻¹
vwind	meridional wind	m s ⁻¹
rh	relative humidity	%

2.5 Statistical Parameters

For the purpose of directly comparing the models to the measurement data, linear interpolation needed to be performed between the individual data points of the models to get information about the altitudes at which the radiosondes have measured. After that, the difference between model data and measurements could be calculated ($\Delta = \text{sonde} - \text{model}$). A positive Δ means the modeled value is smaller so the

measurement was underestimated. Therefore a negative Δ implies overestimation. Afterwards, these results were plotted in different ways for evaluation. Additionally, some statistical parameters have been computed to quantify the accuracy of the models which are explained in this section.

First, there is the mean or average of a set of values. It is calculated by dividing the sum of all values by their quantity. If the data set is sorted by size, the middle value can be determined which is called the median,

$$med = \begin{cases} x_{\frac{N+1}{2}} & \text{if } N \text{ is odd,} \\ \frac{x_{\frac{N}{2}} + x_{\frac{N}{2}+1}}{2} & \text{if } N \text{ is even} \end{cases} \quad (2.5)$$

where N is the sample size and x the sample value.

The median is not useful in comparing the absolute values but when analyzing the difference between measurement and simulation which can be plotted in histograms showing the relative frequency of the deviations categorized in discrete bins. If comparing the median to the mean of that data set, it can be useful to determine if the distribution is symmetrical or not. For a normal distribution (Gaussian distribution) the difference between mean and median would be zero since it is defined as being equally distributed around its mean. In this case both values would have the same amount.

A common parameter to identify the extent of dispersion around the mean value is the standard deviation (STD) σ ,

$$\sigma = \sqrt{\frac{1}{N-1} \cdot \sum (x'_i)^2} \quad (2.6)$$

where x' is the difference between the value x and the sample mean value \bar{x} . A large standard deviation would imply a lot of scattering around the average and vice versa.

Another way to check if a distribution is normally distributed is the kurtosis κ . It provides information on the tail extremity - thus the outliers of a distribution (Westfall, 2014). A negative kurtosis means less outliers compared to a normal distribution which is called platykurtic while a positive kurtosis implies more outliers. This case is called leptokurtic. If a distribution is gaussian, it is called mesokurtic (Pearson, 1905). Pearson defines the mesokurtic case as $\kappa = 3$. In this thesis Fisher's definition is used where three is subtracted from the equation so a normal distribution would give $\kappa = 0$.

Apart from a frequency distribution, another way of evaluating data accuracy is to plot reference set and test set against each other and perform a linear regression. In the ideal case, the relation should be 1:1. This rarely happens, so in addition to slope and standard deviation, the coefficient of determination R^2 helps to identify

how accurate a regression model is - here always a linear model. It describes the proportion of variance explained by the model. The value is always between zero and one, whereby one means 100% variance is explained.

Chapter 3

Results

The parameters presented in the previous Section are listed in the subsequent tables in order to be able to refer to them in the following. Shown is always the deviation from the radiosonde, i.e. Delta Δ , as defined in Section 2.5.

Table 3.1: Parameters presented in Section 2.5 for ECMWF calculated for each considered variable. The units are hPa, °C, m s^{-1} , m s^{-1} , m s^{-1} and % in that order. Kurtosis is dimensionless. The maximum corresponds to the value of left edge of the bin with the highest relative frequency.

	p	T	u	v	U	RH
mean	0.09	0.28	-0.04	-0.19	0.21	-6.57
median	0.34	0.26	-0.03	-0.14	0.24	-1.83
range	27.06	16.56	37.03	33.88	28.53	190.19
STD	1.68	0.96	2.70	2.66	2.56	16.26
kurtosis	22.91	2.52	3.33	2.35	1.91	3.70
maximum	0.27	0.25	-0.24	0.00	0.60	-0.99

Table 3.2: like Table 3.1 but for GDAS

	p	T	u	v	U	RH
mean	-1.18	-0.10	-0.21	-0.42	0.30	-10.39
median	-0.91	-0.07	-0.08	-0.39	0.34	-6.07
range	31.00	18.76	36.72	31.47	36.01	184.36
STD	1.43	1.09	2.92	2.78	2.85	18.77
kurtosis	11.73	2.91	1.86	1.54	1.86	1.86
maximum	-0.50	-0.05	-0.12	-0.24	-0.12	-0.46

3.1 Pressure

The first examined variable is air pressure p . The scatter plot shown in Figure 3.1 proves, that pressure modelling is rather reliable. The data points are barely visible behind the fitted linear regression line which means there is only very limited scattering. In fact, 100 % of scattering is explained by the regression model ($R^2 = 1$)

for both models. For ECMWF the slope is one as well, while it is a little higher for GDAS, although standard deviation looks a bit better for that model. Please note, that standard deviations shown in the scatter plots refer to the absolute values while in Tables 3.1 and 3.2 it refers to the deviation from the mean difference between the values.

On closer inspection, it can be seen that the deviation is a little larger for higher pressure values. One reason for that could be the height correction performed for ECMWF since surface altitude above MSL considered by this model differs slightly from the one used at TROPOS. That is because the model calculates profiles for a grid point (9 x 9 km) while the institute can use the exact height above MSL at their location.

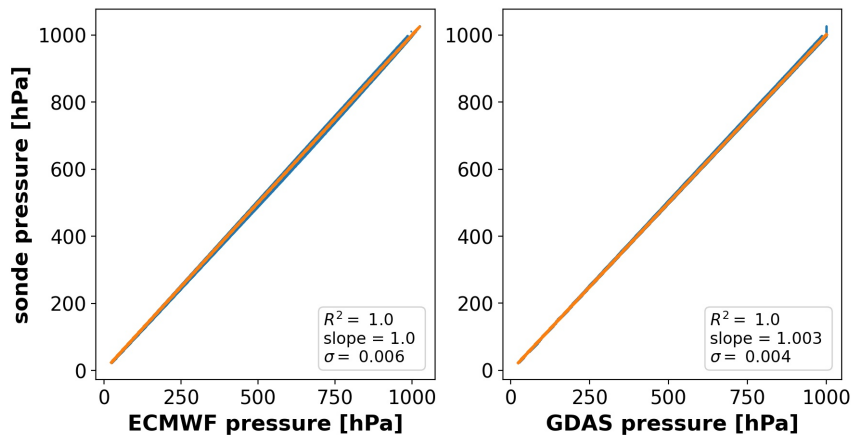


Figure 3.1: 1:1 scatter plot (blue) of radiosonde measurements of pressure and interpolated model data for ECMWF (left) and GDAS (right) with linear regression fit (orange) and calculated R^2 , slope and σ .

The distribution of the differences between measurements and modelled data are shown in Figure 3.2 with respect to their relative frequency. The differences between the models regarding pressure become a lot more visible here. ECMWF displays a positive bias, while GDAS on the other hand shows a negative bias. Both can be confirmed by the mean values as well as the medians (see Tables 3.1 and 3.2). Also, the maximum frequency is significantly lower for GDAS compared to ECMWF. This is due to the fact that the main part of the distribution of ECMWF's values are concentrated much closer around the mean. The range is a little smaller as well but ECMWF shows some outliers which are visible in the histogram between $\Delta p = -2.5$ hPa and -11 hPa. That means larger deviations from measurements happen more often compared to GDAS which leads to a much higher kurtosis and a bigger STD.

The reason behind the high range of the GDAS distribution can not be explained with this histogram because the frequency of these outliers is so low, they don't show up in the graph. Another conspicuity in the GDAS distribution are the two smaller peaks between $\Delta p = -2.5$ hPa and -5 hPa. The origin of these can be explained by

the two dimensional histogram (Fig. 3.3). With increasing height, the histogram takes on a pretty distinct shape. This is due to linear interpolation and the fact, that the distance between data points increases with altitude. Representing a curve with straight lines between the data points works increasingly poorly the further the points are apart, if an exponential decrease is observed. At about 15 km and 18 km altitude, brighter spots (meaning higher relative frequencies) can be seen that differ significantly more from zero compared to the rest of the plot. These are probably the reason for the two additional peaks in the previously discussed histogram. It becomes obvious that the method of linear interpolation is a main reason for the broad distribution of GDAS and presents a significant source of error in this case.

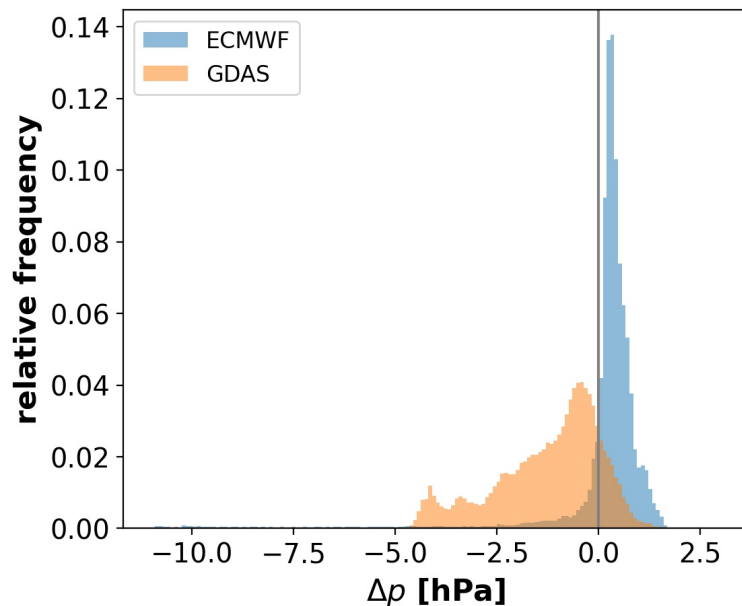


Figure 3.2: Histogram of the difference between pressure measured by the radiosondes and modelled, interpolated data for ECMWF (blue) and GDAS (orange). The data was divided into 150 bins and weighted to get the relative frequency of each bin. Additionally, a vertical line at $\Delta = 0$ was plotted for better visualization.

Looking at the left panel where the pressure difference for ECMWF is depicted, the mentioned problem with linear interpolation does not become visible because the data points are much closer together since there are a lot more of them than in the other model. Also, the deviations become smaller with higher altitudes which leads to an increase in relative frequency. The outliers mentioned before are clearly visible in this graph as well and it looks like they belong to whole profiles, not individual values that differ from the rest.

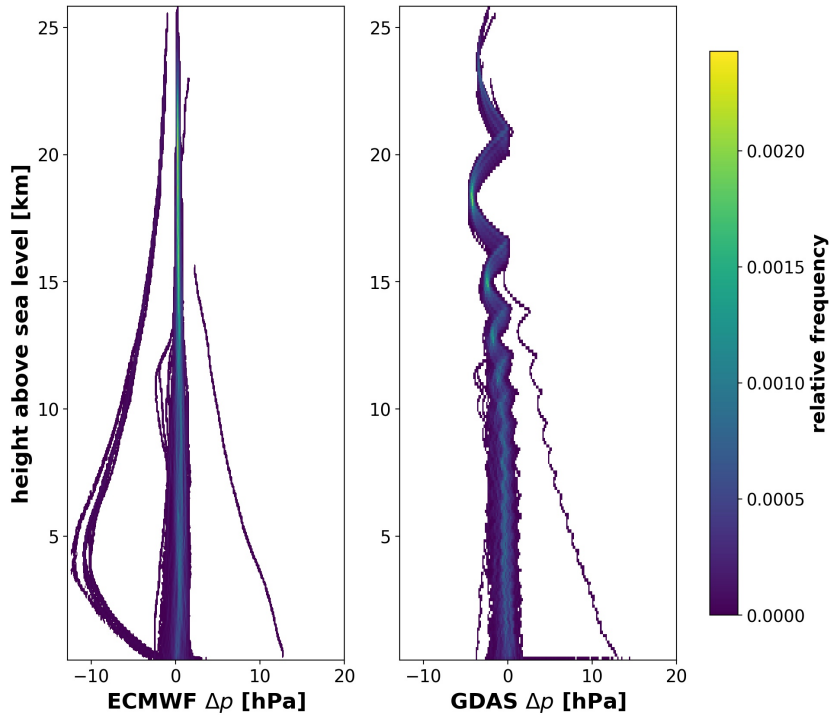


Figure 3.3: Two dimensional histograms of pressure for ECMWF (left) and GDAS (right) with respect to the height above mean sea level in km. The relative frequency is depicted via the color bar on the far right.

3.2 Temperature

In this Section the modelling of temperature T will be analyzed. There is quite a bit more scattering visible in Figure 3.4 compared to the 1:1 plot of pressure but standard deviation is still pretty low. Slope and coefficient of determination are pretty close to one for both models as well, although ECMWF shows a little lower slope which suggests overestimation.

In both panels one distinct artifact is visible where the measured temperature increases while the simulated T remains constant. This occurrence belongs to a single profile from the 28. August 2020 (Fig. 3.5) and might be due to sudden stratospheric warming (SSW). Although, this generally occurs in the winter months. Also, they are associated with a complete reversal of the climatological westerly winds (Butler et al., 2017) which could not be observed in the corresponding profile of wind direction. Therefore, an SSW event is an improbable theory. Another possibility might be first smoke from the wildfires in California, e.g. Baars et al. (2021). This would be difficult for the models to foresee and could explain, why they did not show any kind of unusual change in temperature in that area. It is definitely an interesting occurrence and calls for further research. However, since this is a one time anomaly in the considered time period, this profile was taken out of the temperature data set when calculating the statistical parameters (Tables 3.1 and 3.2) because it had a considerable influence on them. Obviously ECMWF and GDAS aren't prepared for uncommon occurrences like this and it would be interesting to look at other times

this happened and analyze model accuracy further in that respect.

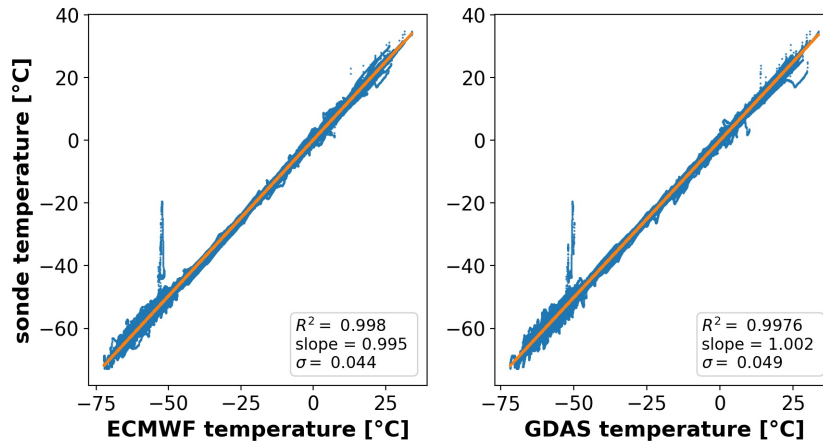


Figure 3.4: 1:1 scatter plot (blue) of radiosonde measurements of temperature and interpolated model data for ECMWF (left) and GDAS (right) with linear regression fit (orange) and calculated R^2 , slope and σ .

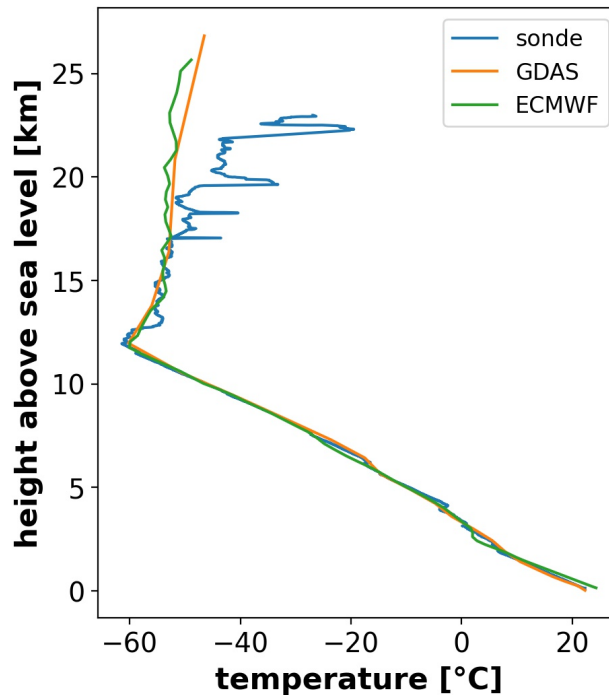


Figure 3.5: Vertical temperature profiles by radiosonde (blue), GDAS (orange) and ECMWF (green) from 28.08.2020

The previously suspected bias in the ECMWF model is not confirmed in the histogram shown in Figure 3.6. Mean, median and the location of maximum frequency are positive which means the predictions are mostly underestimated.

These distributions look a lot more symmetrical compared to pressure. Looking at how similar mean and median are for the two models, this observation is supported. Both are leptokurtic distributions ($\kappa > 0$), meaning heavier tails than a normal distribution would have. A difference between the models is again the maximum frequency which is slightly higher for ECMWF. This leads to a smaller range compared to GDAS.

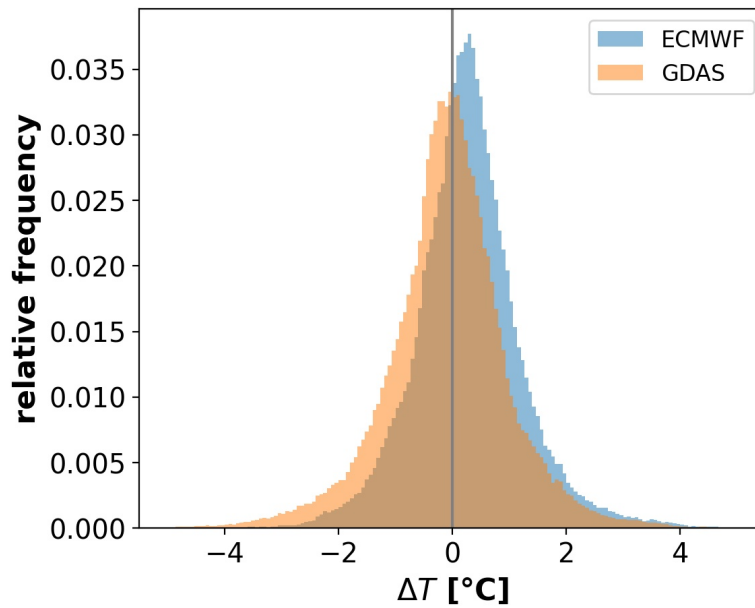


Figure 3.6: Histogram of the difference between temperature measured by the radiosondes and modelled, interpolated data for ECMWF (blue) and GDAS (orange). The data was divided into 150 bins and weighted to get the relative frequency of each bin. Additionally, a vertical line at $\Delta = 0$ was plotted for better visualization.

Taking a look at the two dimensional histograms for temperature (Fig. 3.7), some additional observations can be made: The main one being that there is a visible height dependency. For mid altitudes (between approx. 4 and 11 km), the relative frequency for low differences is noticeably higher and more concentrated around the center than for the rest of the plot. This is probably because temperature decrease is pretty constant in that part of the troposphere. In the atmospheric boundary layer and above the tropopause, temperature tends to be more inconsistent and harder to represent in models. Furthermore, ECMWF seems to have heavier underestimation in high altitudes while GDAS has more outliers at ground level.

One reason for the broader distribution in the lower troposphere and the atmospheric boundary layer are temperature inversions. They are harder to predict accurately by models which can be seen in Figure 3.8. This profile from 25. October 2019 shows a distinct inversion at about 2 km altitude. The models did predict an inversion there but it is clearly visible that the forecast is not perfect. ECMWF got the beginning of the inversion right and the temperature seems to be accurate, as well, but the following temperature increase is too low and the top of the inversion layer is a bit high. GDAS shows similar problems. Temperature increase is even lower and neither the minimum nor the maximum temperature are correct. The first being overestimated, the second underestimated. All in all this is still a pretty good result for inversion strength compared to other profiles where inversions were completely missed. Above the just described inversion, there is another smaller one visible at about 4 km which does not show up in the models at all. Looking at other profiles it becomes obvious that small inversions tend to get over seen by the models while

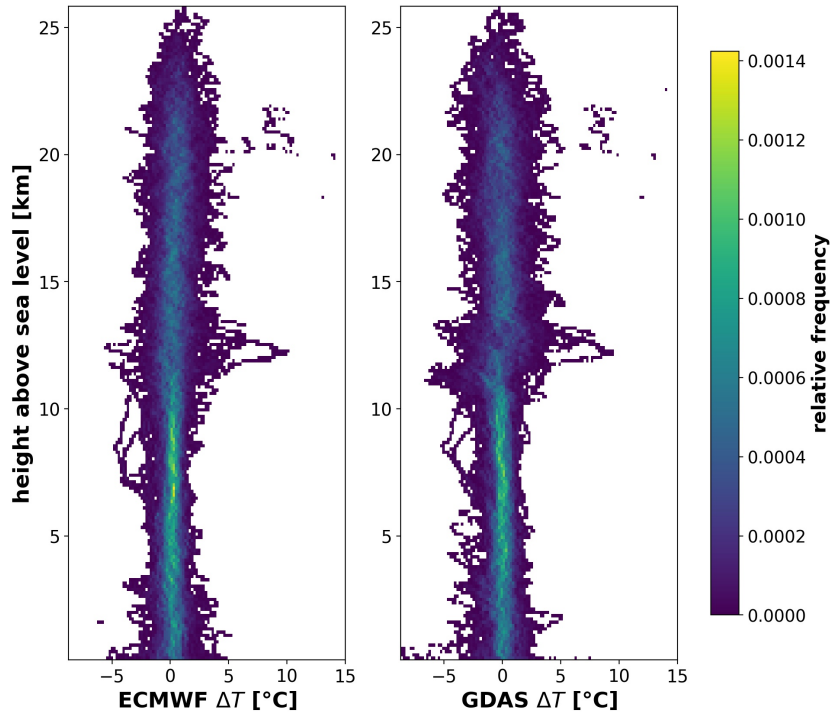


Figure 3.7: Two dimensional histograms of temperature for ECMWF (left) and GDAS (right) with respect to the height above mean sea level in km. The relative frequency is depicted via the color bar on the far right.

larger inversions are predictable but often not very accurately.

Another distinct feature visible in this profile is located at the tropopause inversion layer. The minimum temperature at about 13 km gets a little underestimated (with respect to its amount) by ECMWF but completely missed by GDAS since it lies exactly between two height level points. This happens quite frequently and can explain the two peaks between 10 and 15 km on the left hand side of the distribution of the two dimensional histogram created for the temperature deviations of GDAS (Fig. 3.7, right panel). In accordance to that, the relative frequencies around zero in the same height range are clearly lower.

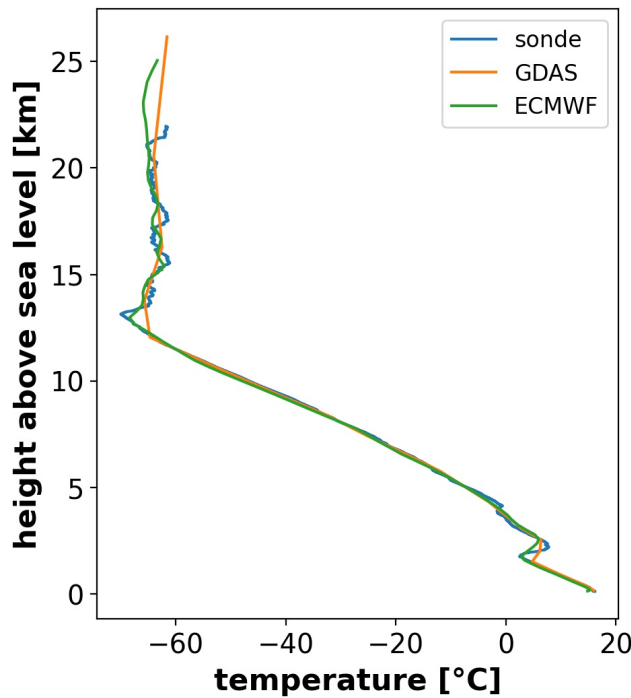


Figure 3.8: Vertical temperature profiles by radiosonde (blue), GDAS (orange) and ECMWF (green) from 25.10.2019.

3.3 Wind Velocity

This Section takes a look at the horizontal wind components u and v as well as the absolute wind velocity U .

3.3.1 Zonal Component u

Wind is again a bit more difficult to model because sudden fluctuations are hard to predict. Looking at the 1:1 plot (Fig. 3.9), even more scattering and outliers are visible but all in all the results are still pretty solid for the zonal wind component. ECMWF again presents slightly better standard deviation and R^2 but its slope is a bit lower compared to GDAS and therefore further away from 1. Both models show a wider spread in the middle part of the plot but that could be explained by the fact that high velocities did not occur as often in the considered time period. On the other hand, low velocities are not rare.

The histograms (Fig. 3.10) again show quite symmetrical distributions. While for ECMWF median and mean are pretty close together, the maximum on the other hand differs quite a bit, although all of the values are negative suggesting a slight overestimation. Mean and median are a bit further apart for GDAS, but the maximum lies in between. Again, all three values are negative. Kurtosis is pretty low for both models especially compared to temperature and pressure. The maximum frequency is lower as well so that the 65% percentile ($\bar{x} \pm \sigma$) is wider than

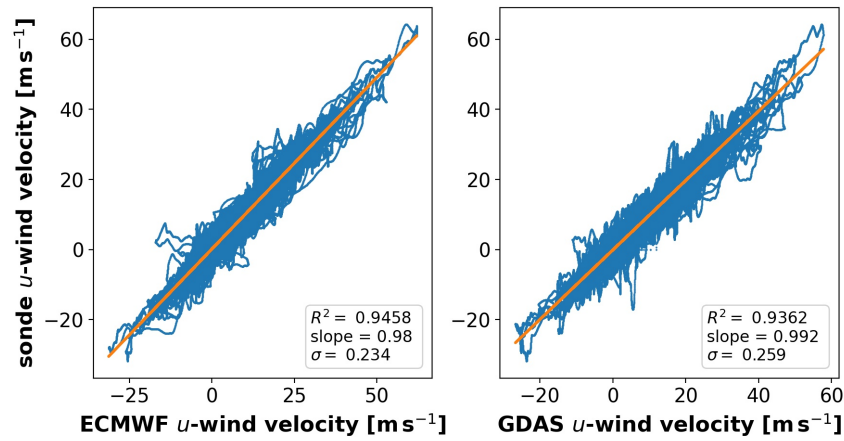


Figure 3.9: 1:1 scatter plot (blue) of radiosonde measurements of zonal wind and interpolated model data for ECMWF (left) and GDAS (right) with linear regression fit (orange) and calculated R^2 , slope and σ .

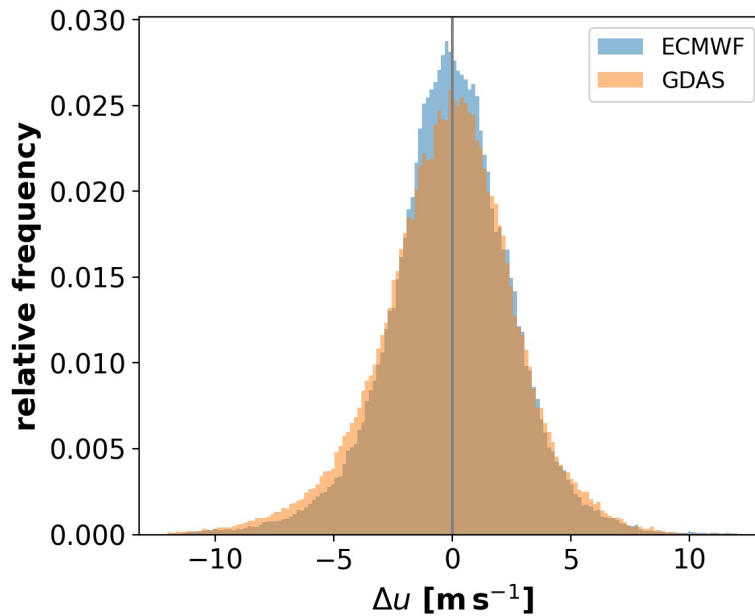


Figure 3.10: Histogram of the difference between zonal wind measured by the radiosondes and modelled, interpolated data for ECMWF (blue) and GDAS (orange). The data was divided into 150 bins and weighted to get the relative frequency of each bin. Additionally, a vertical line at $\Delta = 0$ was plotted for better visualization.

for temperature. The standard deviation proves this, which is considerably larger than for the previously discussed variables.

The two dimensional histogram (Fig. 3.11) does not show a visible height dependency for Δu . The only thing that could be said is that there seem to be larger outliers for mid altitudes between about 5 and 15 km. Also, relative frequency is a bit higher closer to the ground until about 10 km.

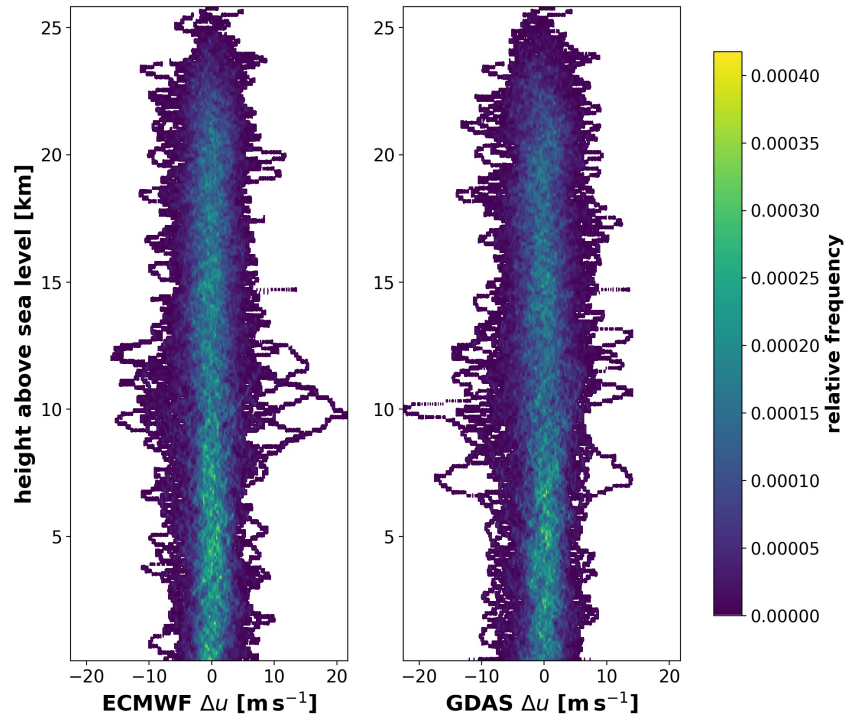


Figure 3.11: Two dimensional histograms of the zonal wind for ECMWF (left) and GDAS (right) with respect to the height above mean sea level in km. The relative frequency is depicted via the color bar on the far right.

3.3.2 Meridional Component v

The results for the meridional component of the horizontal wind vector are quite similar to u . One difference is the slope of GDAS which is larger than one now (see Fig. 3.12). The overestimation is also more visible in the histogram for GDAS (Fig. 3.13), as the distribution has a larger area on the left hand side of zero. Again, ECMWF reaches higher relative frequencies which leads to a lower standard deviation compared to GDAS. Although, the difference is smaller than for u .

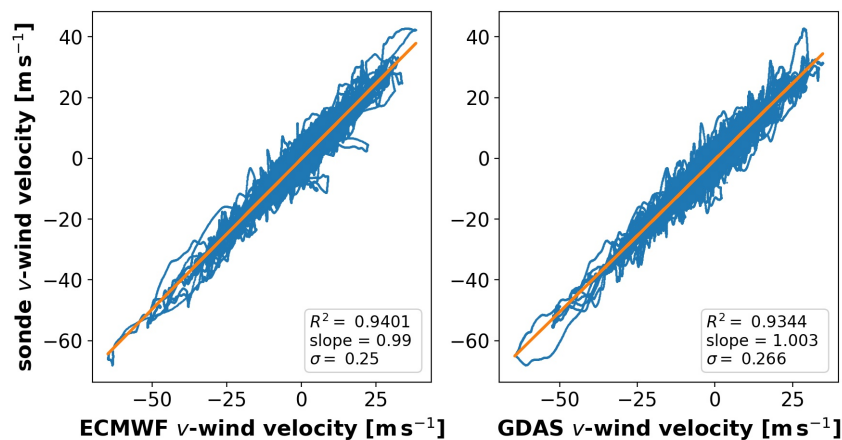


Figure 3.12: 1:1 scatter plot (blue) of radiosonde measurements of meridional wind and interpolated model data for ECMWF (left) and GDAS (right) with linear regression fit (orange) and calculated R^2 , slope and σ .

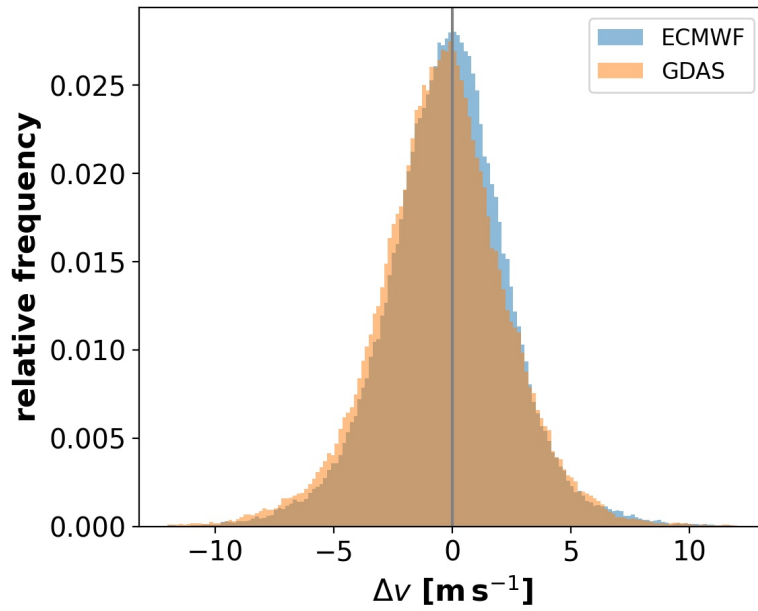


Figure 3.13: Histogram of the difference between meridional wind measured by the radiosondes and modelled, interpolated data for ECMWF (blue) and GDAS (orange). The data was divided into 150 bins and weighted to get the relative frequency of each bin. Additionally, a vertical line at $\Delta = 0$ was plotted for better visualization.

3.3.3 Absolute Wind Velocity U

The 1:1 plot of the absolute wind velocity U (Fig. 3.14) shows similar results as for u and v . It can be seen that scattering around the 1:1 line is higher for small velocities and getting less for higher velocities. For ECMWF, the slope is a bit lower compared to u and v . This is because U is calculated from its components. Since they already show a positive bias in slope, the resulting bias is a little higher due to error propagation. The same behaviour is found for GDAS.

The corresponding histogram 3.15 shows a positive bias for both ECMWF and GDAS (underestimation). Here, the maximum relative frequency for ECMWF is again significantly higher.

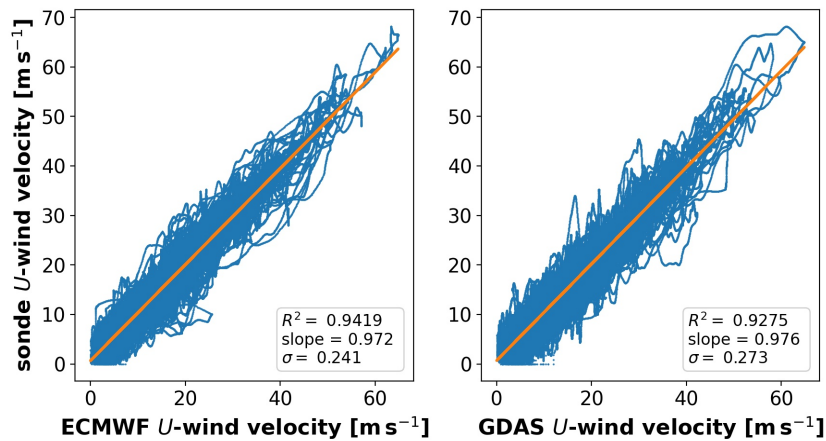


Figure 3.14: 1:1 scatter plot (blue) of radiosonde measurements of absolute wind velocity and interpolated model data for ECMWF (left) and GDAS (right) with linear regression fit (orange) and calculated R^2 , slope and σ .

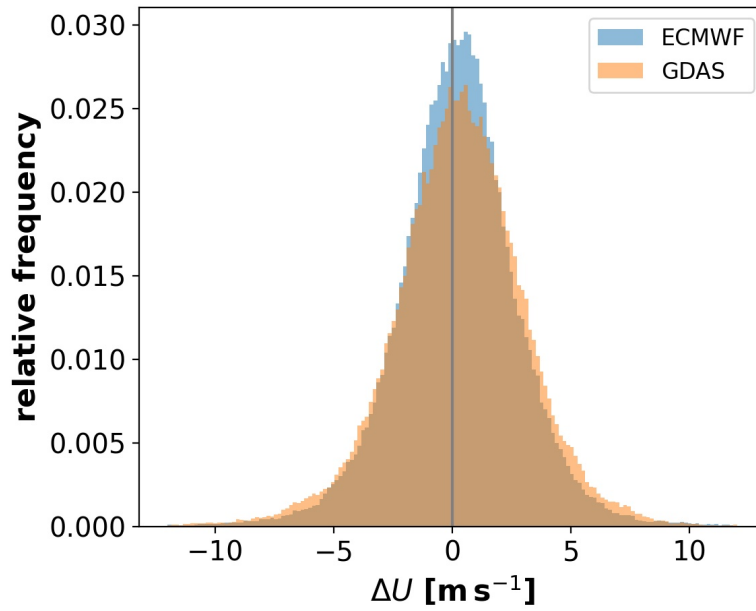


Figure 3.15: Histogram of the difference between absolute wind velocity measured by the radiosondes and modelled, interpolated data for ECMWF (blue) and GDAS (orange). The data was divided into 150 bins and weighted to get the relative frequency of each bin. Additionally, a vertical line at $\Delta = 0$ was plotted for better visualization.

3.4 Wind Direction

In this section, wind direction α of the models and radiosonde will be analyzed. It is a bit more difficult to compare measurements and simulations directly, especially for northerly wind since wind direction is described by a circle. For example, if the radiosonde measures 358° and the model says 2° , the simulation is pretty close to the truth in a physical sense but the mathematical difference is huge. This problem can be seen in Figure 3.16. Most data points lie on or somewhere around the 1:1 line, although scattering is quite significant. In the top left and bottom right corners of both plots, distinct areas are visible that have nothing to do with outliers but with the previously described problem. This is why no linear regression has been performed because it would distort the results of slope, R^2 and σ considerably. This is also the reason why histograms of deviations are not shown for this parameter. The ranges of both histograms are almost $2 \cdot 360^\circ$ wide but this is not necessarily representative for the model accuracy.

The two dimensional histograms depicted in Figure 3.17 show a clear height dependency for the accuracy of modelling wind direction. The best results are to be found in the upper troposphere and lower stratosphere. The distribution is a bit broader near the ground. One possible reason is that the local wind direction might be influenced by trees and buildings leading to fluctuations that are not predictable by the models. The deviations in the troposphere (above 15 km) are even higher. This will be analyzed in the following section.

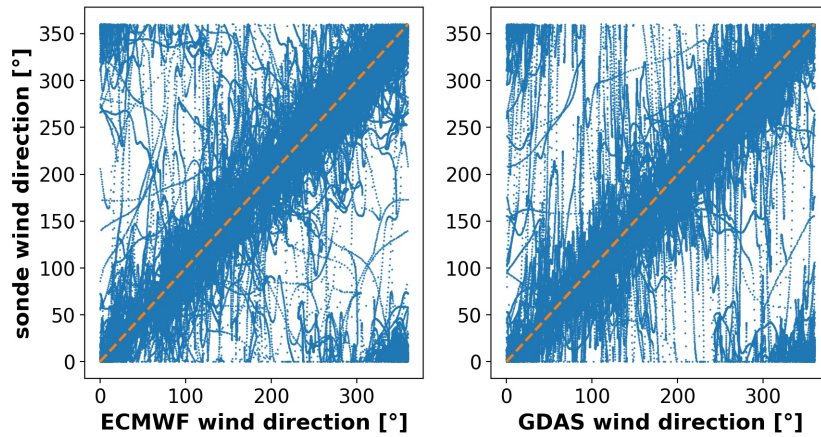


Figure 3.16: 1:1 scatter plot (blue) of radiosonde measurements of wind direction and interpolated model data for ECMWF (left) and GDAS (right) with ideal 1:1 line (dashed, orange).

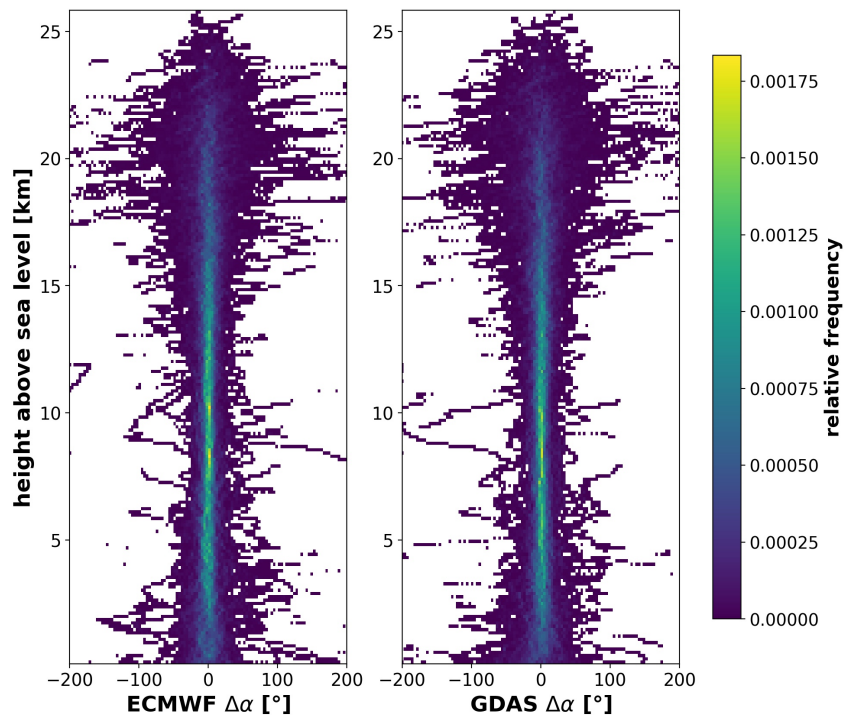


Figure 3.17: Two dimensional histograms of wind direction for ECMWF (left) and GDAS (right) with respect to the height above mean sea level in km. The relative frequency is depicted via the color bar on the far right.

3.5 Wind Case Examples

The previously mentioned large deviations above 15 km altitude may be explained by the example case from 19. July 2019 shown in Figure 3.18. In the troposphere, the wind direction changes from westerly to easterly wind. In between these layers, wind direction varies a lot and in very small height intervals as well. One time even 360° in less than one kilometer. The change to easterly wind is predicted by the models, however their resolution is too low to forecast these strong and rapid changes. Especially GDAS has problems in that area since its height levels are so far apart. To put this profile into context with wind speed, Figures 3.19 to 3.20 can be viewed. The agreement looks pretty good as was already observed in the 1:1 plots

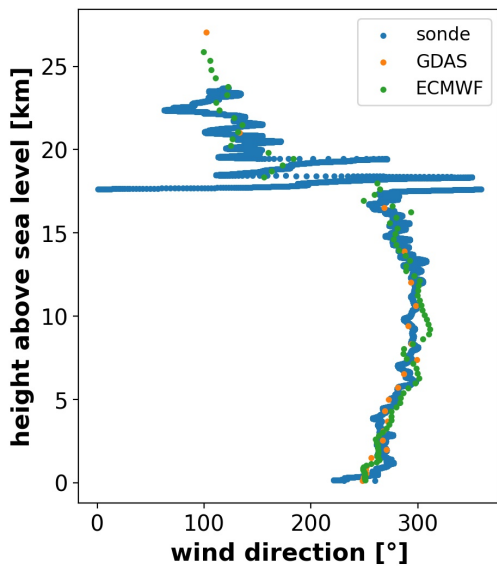


Figure 3.18: Vertical profiles of wind direction from 19.07.2019.

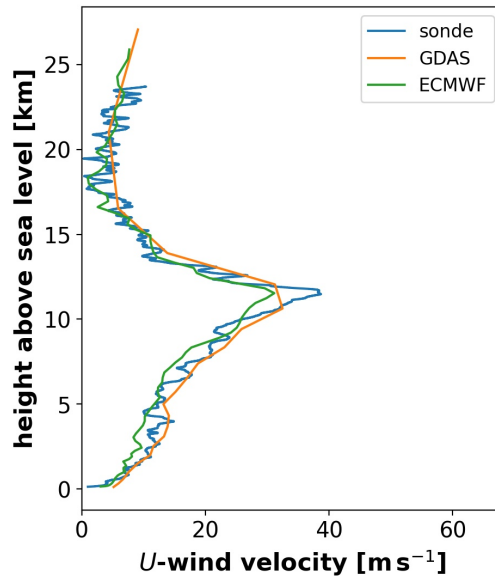


Figure 3.19: Vertical profiles of wind speed from 19.07.2019.

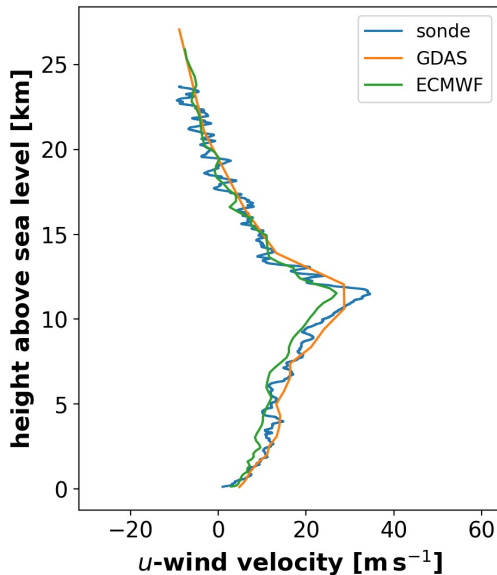


Figure 3.20: Vertical profiles of zonal wind from 19.07.2019.

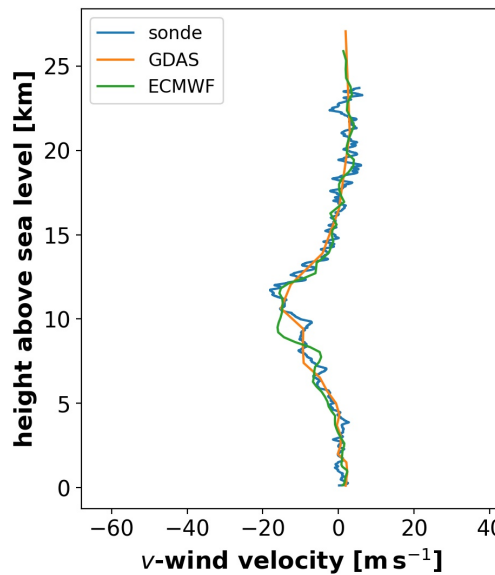


Figure 3.21: Vertical profiles of meridional wind from 19.07.2019.

and histograms. A couple of things can be derived anyway. Below 15 km westerly wind is predominant which leads to a rather low v component (Fig. 3.21) and a positive u component. In the area between 17 and 19 km, where the wind direction changes a lot, the measured wind velocity U (Fig. 3.19) is very low. This leads to a low u and v with changing sign. For ECMWF, these fluctuations were predicted as well but not as rapid and small scaled as it was measured. One reason for this is the lower resolution. This problem is even bigger for GDAS.

As was observed in the temperature profiles before, GDAS has trouble with predicting maxima (or minima) of wind as well if they are located between two levels. This can be seen in Figures 3.19 and 3.20 at about 11 km. In ECMWF this peak is visible but was massively underestimated.

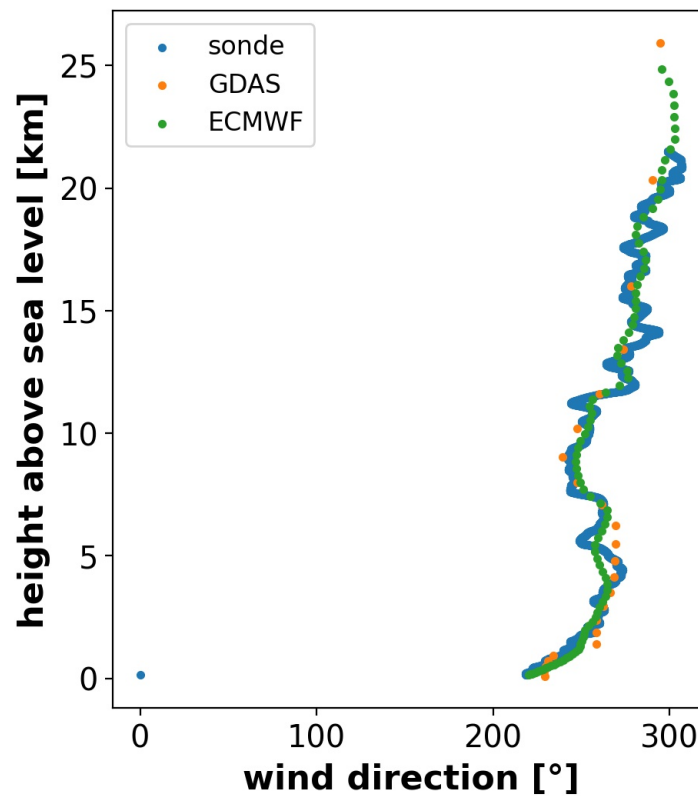


Figure 3.22: Vertical profiles of wind direction from 04.02.2022

Of course this change from westerly to easterly wind does not happen every day, but the discussed profile isn't the only one where it can be seen. Thus, this phenomenon might be one valid reason for the intense deviations above 15 km seen in Figure 3.17. Low differences close to zero generally occur when the wind direction is relatively constant in height. This can already be derived from Figure 3.18 since below 15 km mainly westerly wind has been detected. For confirmation Figure 3.22 can be viewed as well. Here, even above 15 km, the wind direction does not change much and the prediction is still quite good. Although small fluctuations are again mostly ignored by the models due to lower resolutions.

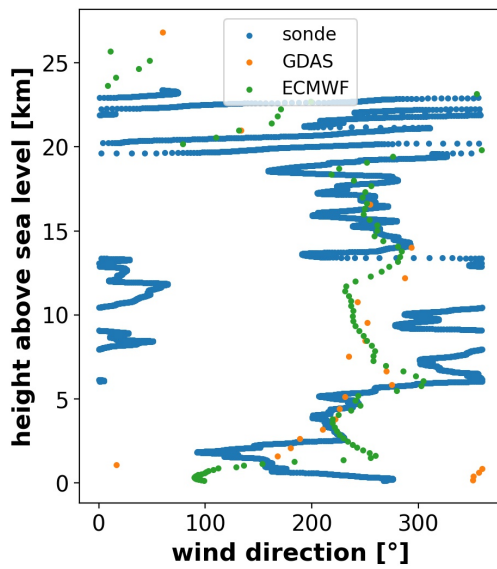


Figure 3.23: Vertical profiles of wind direction from 30.08.2019.

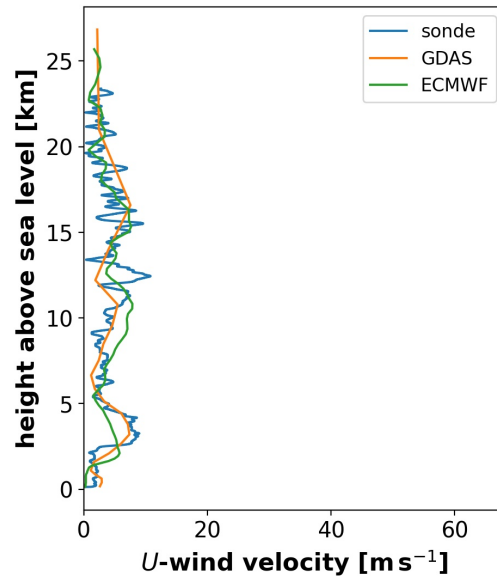


Figure 3.24: Vertical profiles of wind speed from 30.08.2019.

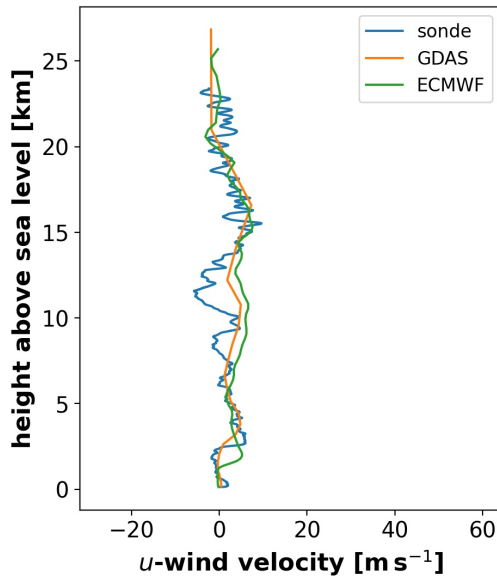


Figure 3.25: Vertical profiles of zonal wind from 30.08.2019.

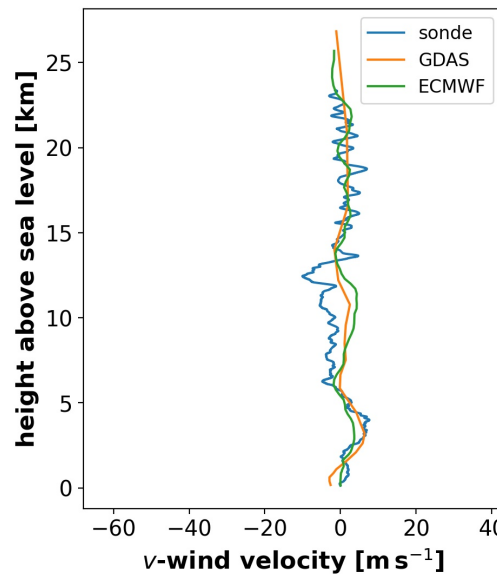


Figure 3.26: Vertical profiles of meridional wind from 30.08.2019.

As could be observed in the 1:1 plot (Fig. 3.16) large outliers are pretty common in wind direction. One day where this occurred is the 30.08.2019 shown in Figure 3.23. The measured direction is highly variable and changes a lot in short height intervals. This might be explained by the low wind velocity U on this day which was detected throughout the whole profile (Fig. 3.24). This is due to a stationary front that was stretched across Germany. The ground weather maps created by the German meteorological service (DWD) showing this can be found in the appendix (Sec. 5). As mentioned before, small fluctuations are close to impossible for the models to resolve. This becomes an increasing problem when wind speed is low and leads to the large deviations in the calculated wind direction, especially when combined with under-, or in this case, overestimation of zonal and meridional wind

velocity as can be seen between 8 and 14 km (Figures 3.25 and 3.26).

3.6 Relative Humidity

The last variable to be analyzed is the relative humidity RH . Apart from humidity itself, it gives information about cloudiness. Since radiosondes measure the vertical profile, information about cloud layers on different heights can be derived. This is always a major uncertainty in climate and weather models and the two models considered here make no exception. This is confirmed when looking at Figure 3.27, where the scatter plots of the two models and radiosonde data are displayed. The absolute deviation at low relative humidities is considerably lower. Such low relative humidity generally only occurs in the stratosphere where there barely is any water vapor. The deviations become rather big after RH exceeds 10 % and keep increasing the higher the measured humidity gets. A linear trend still looks to be existent but with the lowest R^2 and highest standard deviation of all variables analyzed in this thesis. Also, it tends to get considerably overestimated as the slope is well below one. Although, it might be mentioned, that ECMWF again delivers a bit better results.

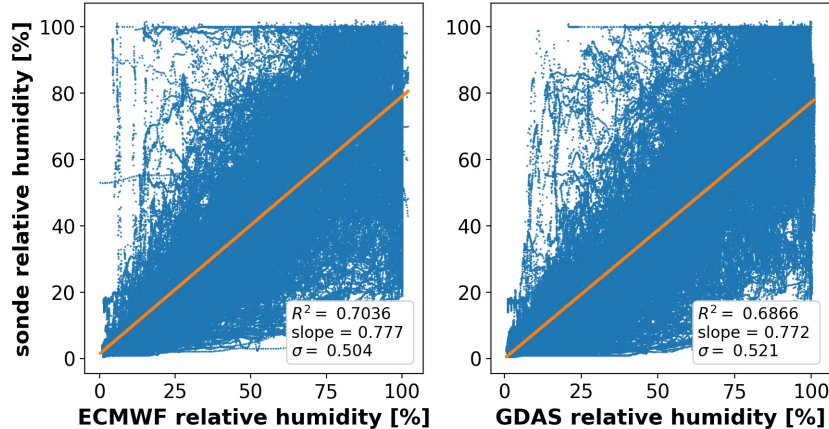


Figure 3.27: 1:1 scatter plot (blue) of radiosonde measurements of relative humidity and interpolated model data for ECMWF (left) and GDAS (right) with linear regression fit (orange) and calculated R^2 , slope and σ .

The corresponding histograms (Fig. 3.28) do not show normal distributions or even symmetrical ones. Though, the maxima are quite close to zero, they are still further away than the maxima of any other variable considered. This is not derivable from the graph because the displayed range is a lot larger than in the previous sections. But the overestimation can be seen clearly, as the proportion of values (or rather bars) below zero is more substantial than above zero. This leads to significantly negative medians and even larger negative mean values in terms of amount. The higher quality of ECMWF is confirmed again as its values are a bit closer to zero. The large standard deviation as stated in the Tables 3.1 and 3.2, is due to the large

difference between the maximum and minimum deviation (range). This leads to a broad range in which the main 65 % lie. This in turn leads to a low kurtosis, though this does not mean the distributions are anywhere near normal.

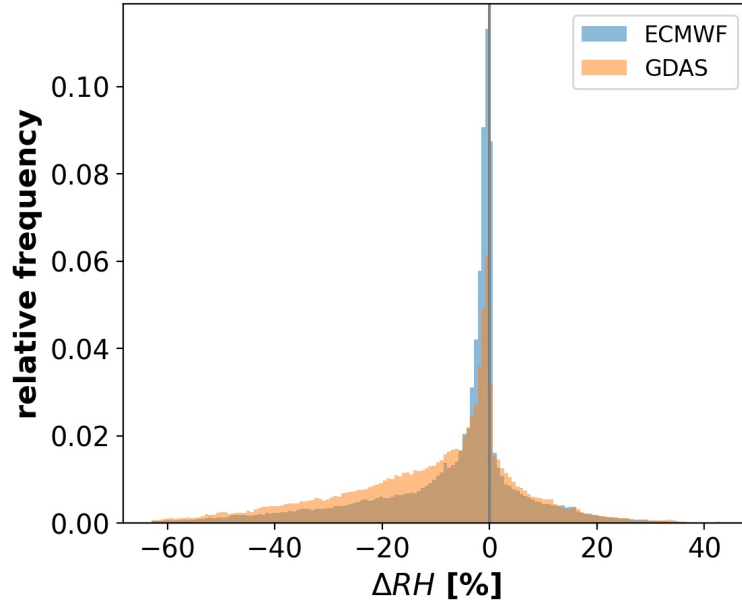


Figure 3.28: Histogram of the difference between relative humidity measured by the radiosondes and modelled, interpolated data for ECMWF (blue) and GDAS (orange). The data was divided into 150 bins and weighted to get the relative frequency of each bin. Additionally, a vertical line at $\Delta = 0$ was plotted for better visualization.

Another distinct feature is the maximum relative frequency. While ECMWF reaches more than 14 %, GDAS only reaches a little over 6 %. The reason for this major discrepancy is not the range of the values but the fact that GDAS does not calculate relative humidity for its upper two levels. This can be seen in Figure 3.29. It is confirmed that good agreement only exists in the stratosphere above about 14 km where humidity is low anyway. This would explain the large but narrow peaks for both GDAS and ECMWF in the histograms (Fig. 3.28) but also the fact, why the maximum of GDAS is a lot lower. There simply are a lot less values. In the troposphere below, the deviations are very prominent. It is also noticeable that the distribution is a bit more centered around zero in the lower troposphere and overestimation gets bigger above 5 km which is where most clouds occur, confirming the trouble models have with them. But it must be said, that the radiosonde is only a point measurement while models give the average over the whole grid point. This definitely needs to be considered in the search for sources of error as well.

The example case from 25. May 2019 shown in Figure 3.30 clearly shows the problem with overestimation mentioned earlier. The thickness of each layer with higher relative humidity was met quite well, though. The first layer with high measured humidity would be the atmospheric boundary layer. GDAS' prediction looks a lot better, although the humidity at ground level was overestimated significantly. Above that the deviations are quite minimal. ECMWF underestimated humidity at ground

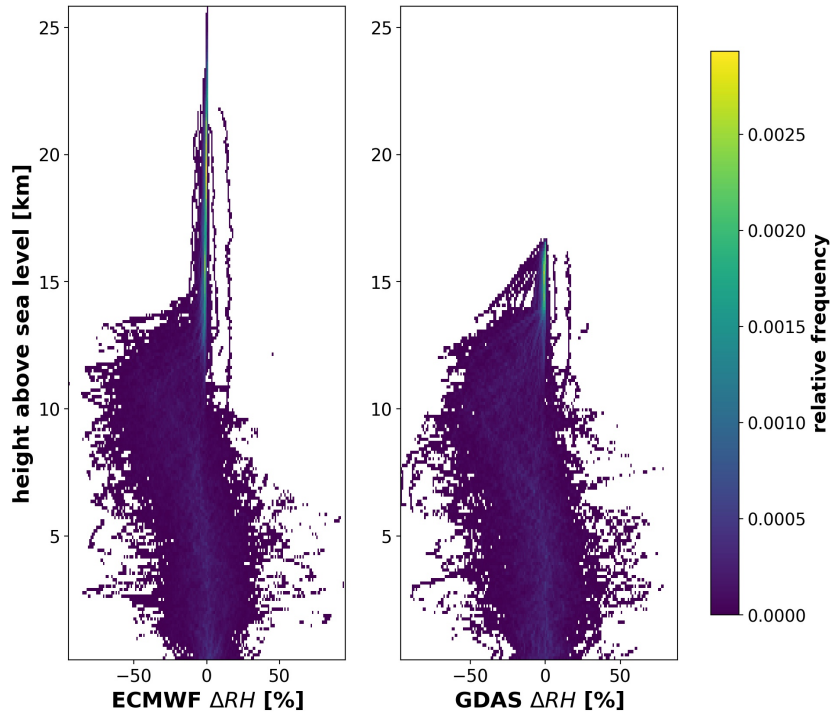


Figure 3.29: Two dimensional histograms of relative humidity for ECMWF (left) and GDAS (right) with respect to the height above mean sea level in km. The relative frequency is depicted via the color bar on the far right.

level a bit and calculated this layer to be higher and more humid. The thickness and location of the second layer was predicted quite well by both models, reaching from about 5 to 12 km. Humidity itself was generally overestimated. GDAS predicted 100% for the whole layer - even more than that at one level. ECMWF shows a little more variation but overestimated as well.

As mentioned before, one reason for deviations can be the point measurement versus the grid point average. This is especially visible for the current case example when looking at the time-height plot of the attenuated backscatter coefficient measured by LIDAR at TROPOS on this day (Fig. 3.31). A thick cloud layer was covering the sky between 13:30 and 16 UTC (high backscattering, indicated by white colors). Then it mostly dissolves at the time of release of the radiosonde. But for GDAS, the time of prediction is 15 UTC. At that time, the cloud layer was still present which proves that a lot can happen within an hour. Also it is possible and probable that the models cannot forecast the exact time a cloud occurs over a location. So even if they predicted 16:30, the humidity would still be pretty high at 16 UTC. Of course this is not the only reason for errors in prediction. All in all this day is a pretty good example for relative humidity.

The RH profile from 10. January 2020 (Fig. 3.32) is an even better example with only minor overestimation between 5 and 10 km and really good agreement in the atmospheric boundary layer. Even the humidity at ground level was predicted quite well.

As discussed before, good agreement is rare for relative humidity. Figure 3.33 shows

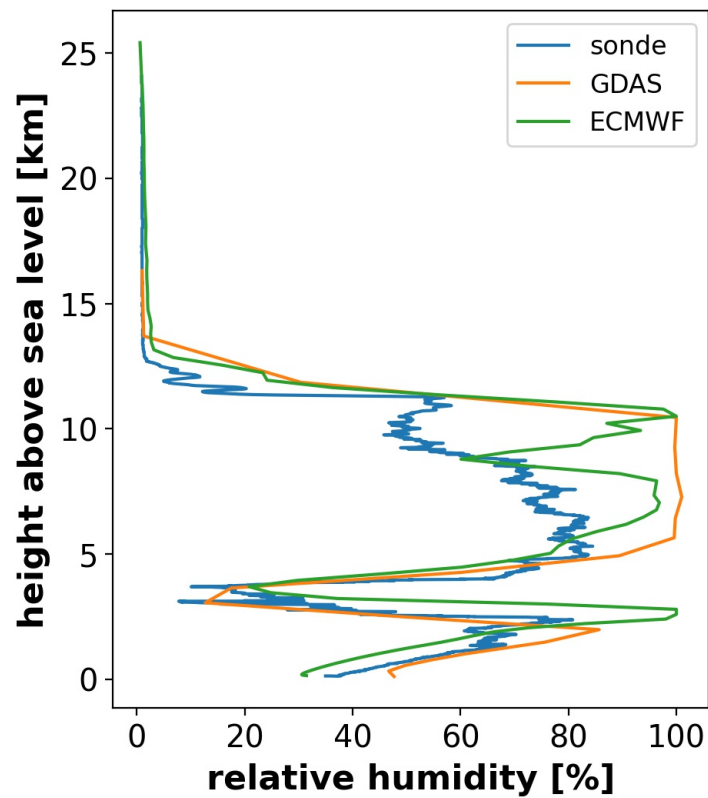


Figure 3.30: Vertical profiles of relative humidity from 24.05.2019

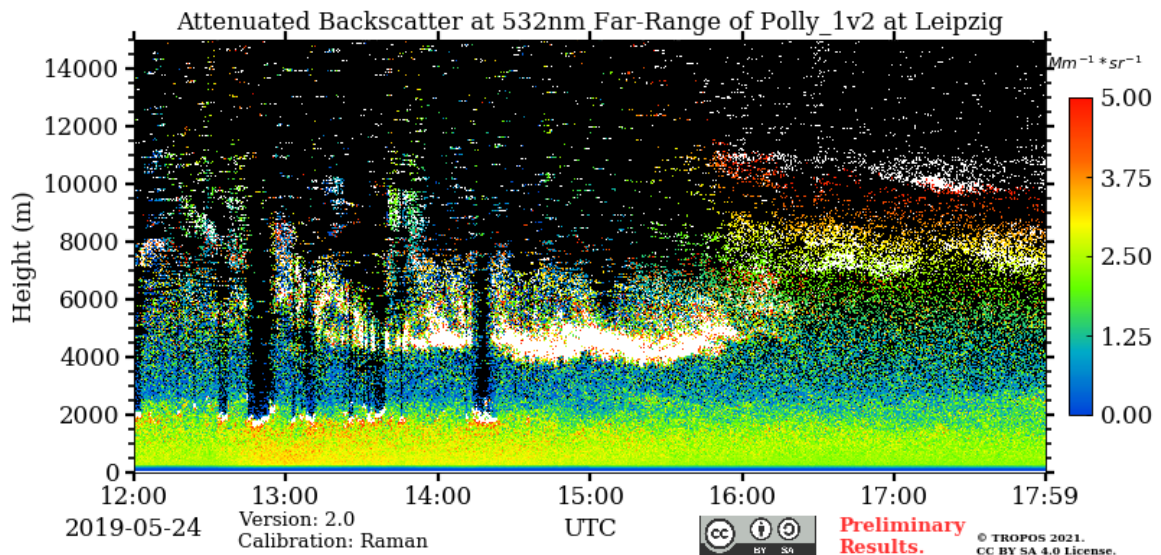


Figure 3.31: Time-height plot of the attenuated backscatter coefficient measured at 532 nm from 24.05.2019 from 12 to 17:59 UTC, measured by LIDAR by the Polly Net station in Leipzig at TROPOS (<http://polly.tropos.de>, accessed: 06.10.2022).

the RH profiles of 6. June 2021. Considerable overestimation for RH between 5 and 12 km is visible. There the measured RH is highly variable. The humidity at ground level was considerably overestimated by both models as well. Even more so by GDAS.

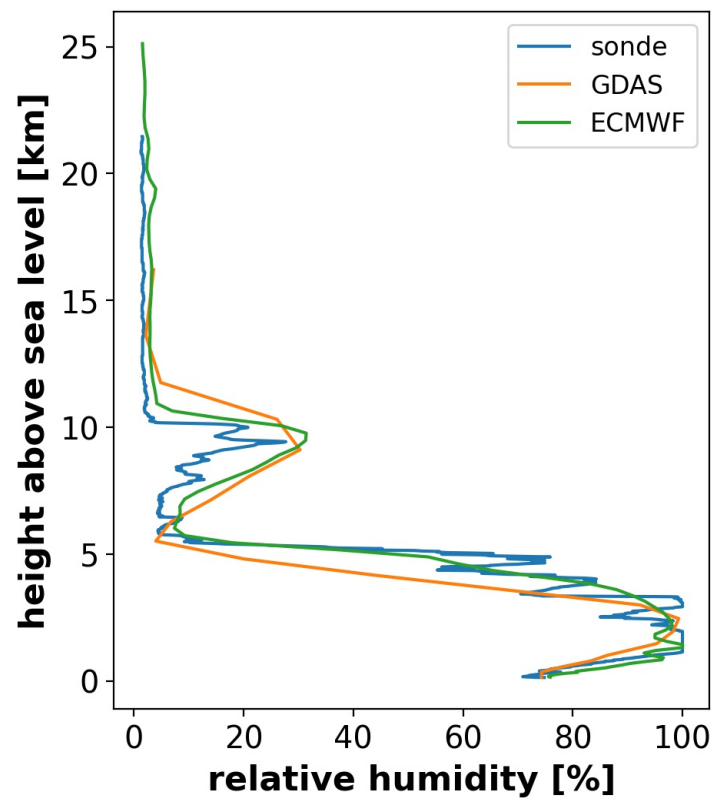


Figure 3.32: Vertical profiles of relative humidity from 10.01.2020

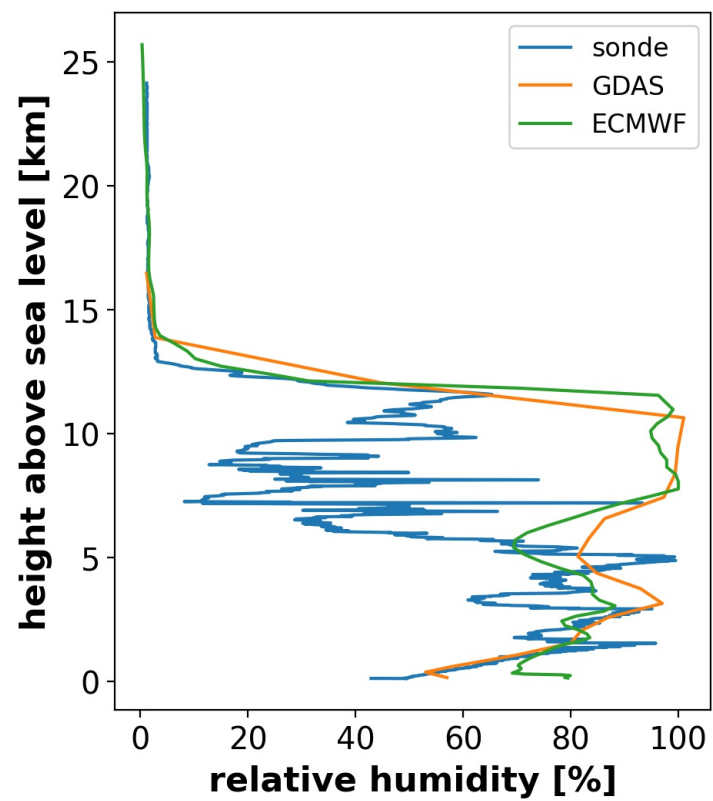


Figure 3.33: Vertical profiles of relative humidity from 04.06.2021

Chapter 4

Summary

The two models considered in this thesis use measurement data of all kinds of observation methods for assimilation and modelling of the standard meteorological variables onto a three dimensional grid. Comparing them to an independent set of radiosonde data that is not provided for the models has led to some interesting conclusions which will be summed up in this chapter.

It could be seen that pressure prediction works well apart from a few outliers. The 1:1 plots have shown very good agreement. Unfortunately, larger deviations occurred for GDAS, especially with low pressure because of linear interpolation. This poses an easy way to make the data comparable but causes problems when the data points are further apart as is the case in GDAS in the stratosphere. ECMWF on the other hand has shown a slight positive bias which implies underestimation.

The models produce good results for temperature as well. Here too, ECMWF exhibited a positive bias but at the same time a smaller range than GDAS which means there are more cases with lower deviations. It was also seen that the accuracy of temperature prediction is dependent of height with the best agreement in the middle and upper troposphere and bigger deviations close to the ground in the atmospheric boundary layer and the stratosphere. The reasons for this are higher variability and more fluctuations that can't be resolved by the models, particularly GDAS. Furthermore, it could be seen that the models tend to ignore anomalies in measurement due to for example wildfires.

Wind velocity is a little harder to predict since it is even more variable. Large peaks in velocity are often over- or underestimated severely by ECMWF or overlooked completely in some cases by GDAS when the peak lies between two levels. All in all the results are still sufficiently accurate to get an overview about what will be happening in the atmosphere. Not being able to resolve small variations in wind speed leads to considerable problems when it comes to wind direction, especially when the velocity is low. The forecasts are better for higher velocities and only minor changes in direction with altitude.

Last but not least, relative humidity was analyzed. This has produced the worst results since it is a highly fluctuating and inconsistent variable, especially if clouds are involved. Both models tend to overestimate humidity significantly. Looking at the profiles, it could be derived that at least the correct profile shape can be observed. For example, a measured increase in humidity due to the radiosonde entering a cloud also shows an increase in predicted humidity although the exact altitude is mostly miscalculated. Humidity forecasts still need to be considered with care which goes for both ECMWF and GDAS. Although, it needs to be taken into consideration - particularly for relative humidity, which isn't just highly variable on a vertical scale but on a horizontal and temporal one as well - that the models produce the grid average while the radiosonde can only measure at one place at a time. So the horizontal resolution and prediction time of a model is important, too.

To summarize the summary, it can be said that models have problems with large fluctuations on a small scale. The higher resolution of ECMWF definitely helped in that respect while GDAS can not resolve some things. So, a higher number of vertical levels is beneficial but to get an overview about the vertical structure of the atmosphere, both models provide good results.

Chapter 5

Appendix

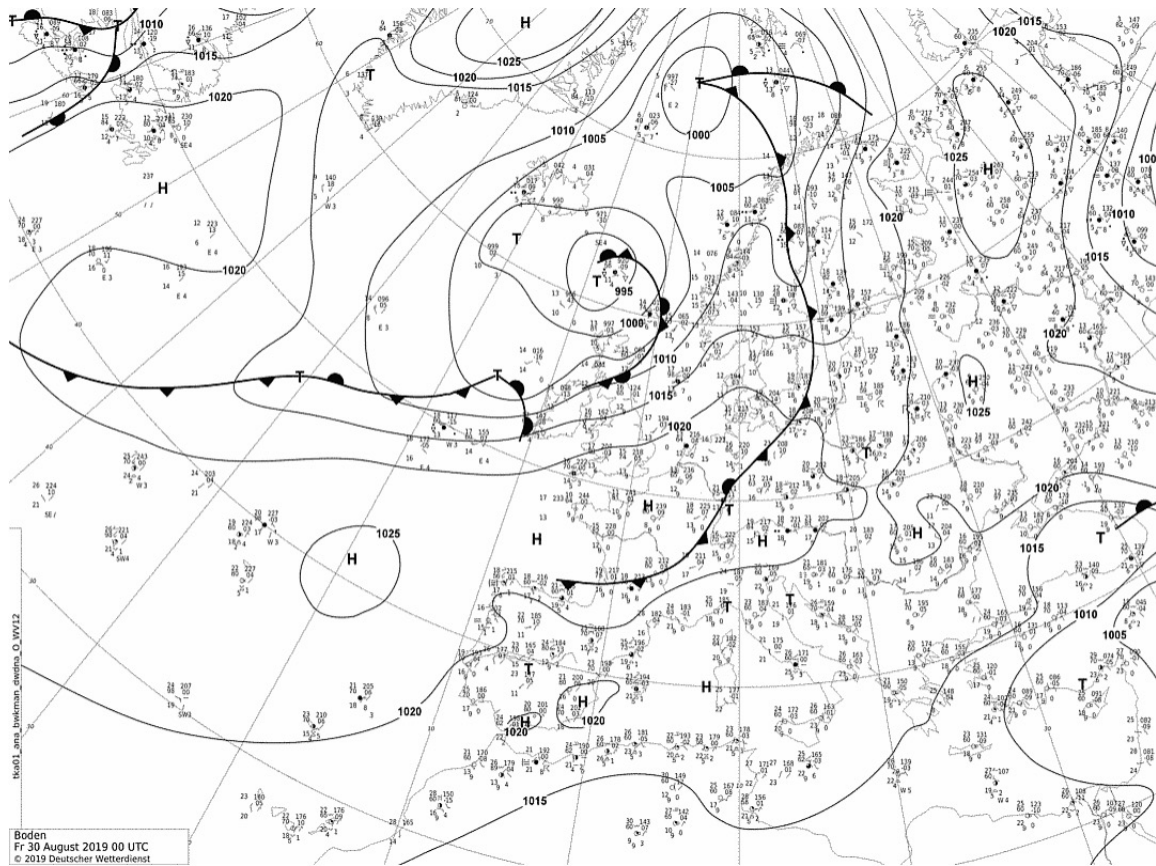


Figure 5.1: front analysis by DWD from 30.08.2019 at 00 UTC (<https://www.wetter3.de>)

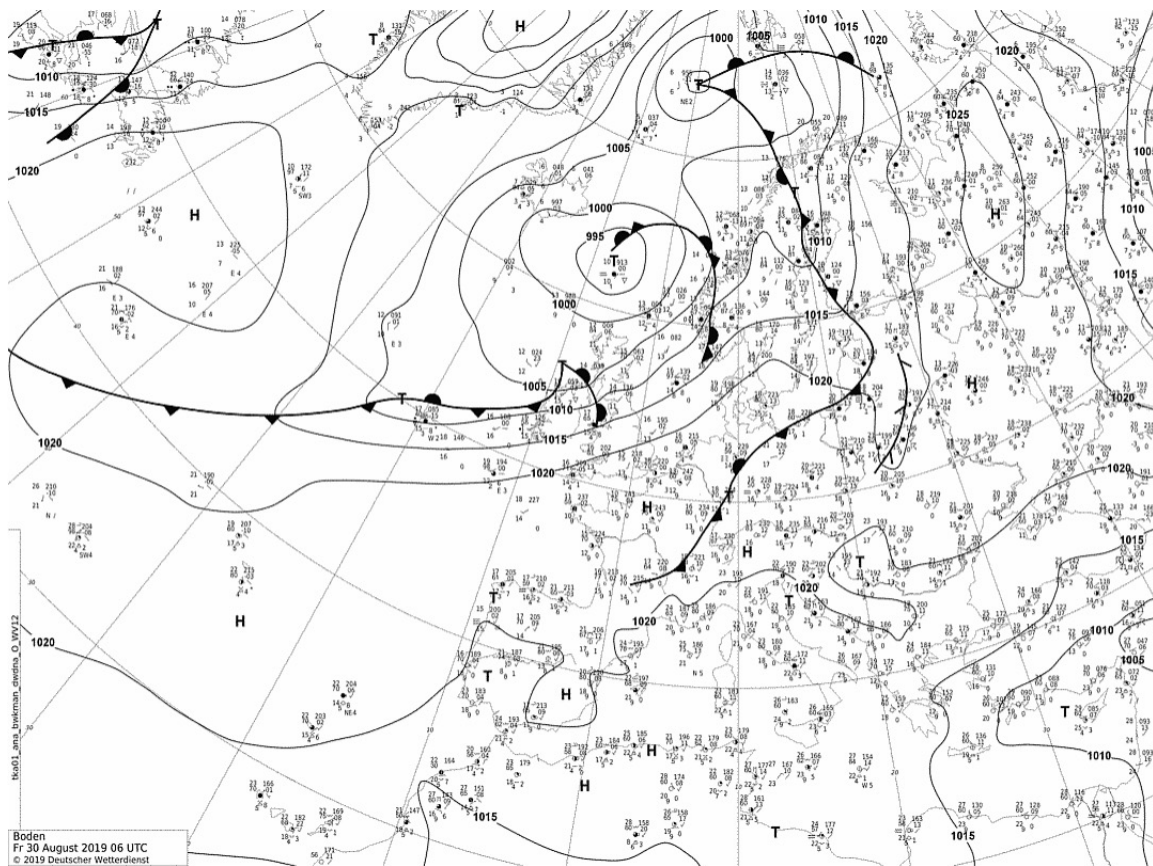


Figure 5.2: front analysis by DWD from 30.08.2019 at 06 UTC (<https://www.wetter3.de>)

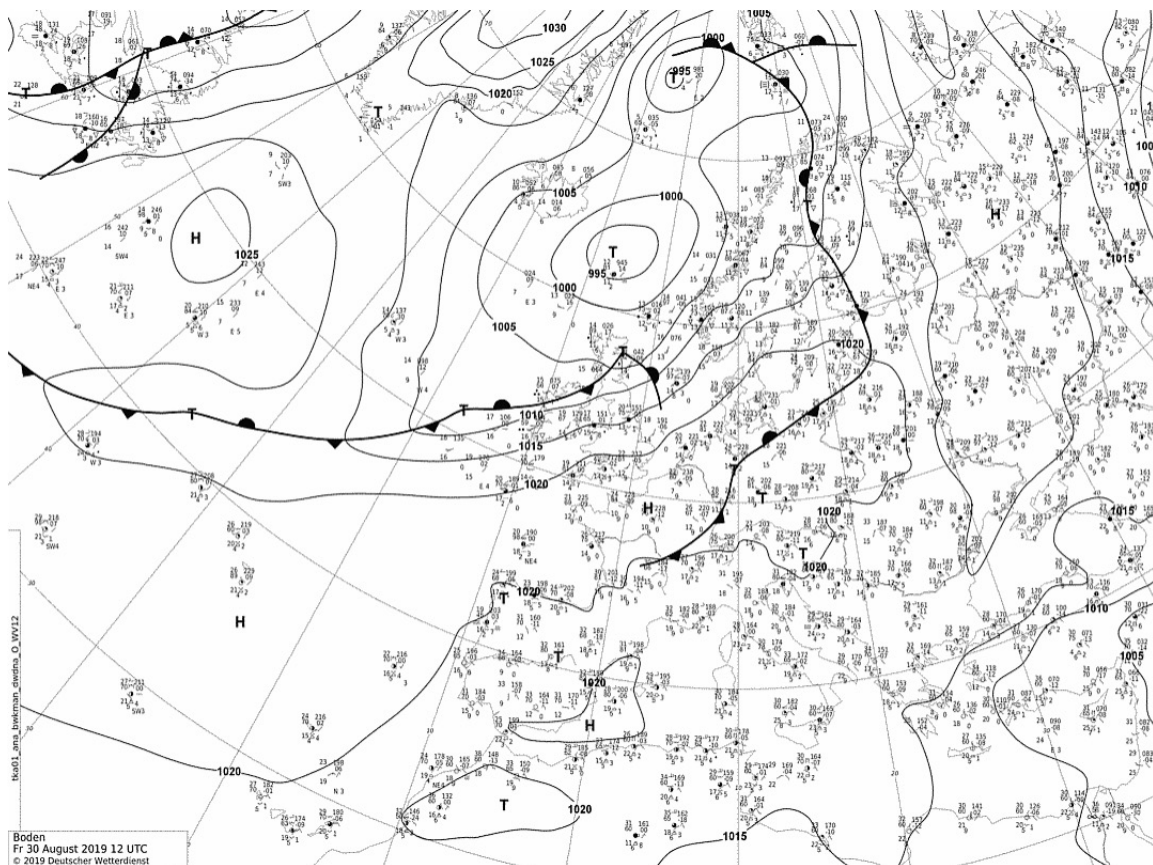


Figure 5.3: front analysis by DWD from 30.08.2019 at 12 UTC (<https://www.wetter3.de>)

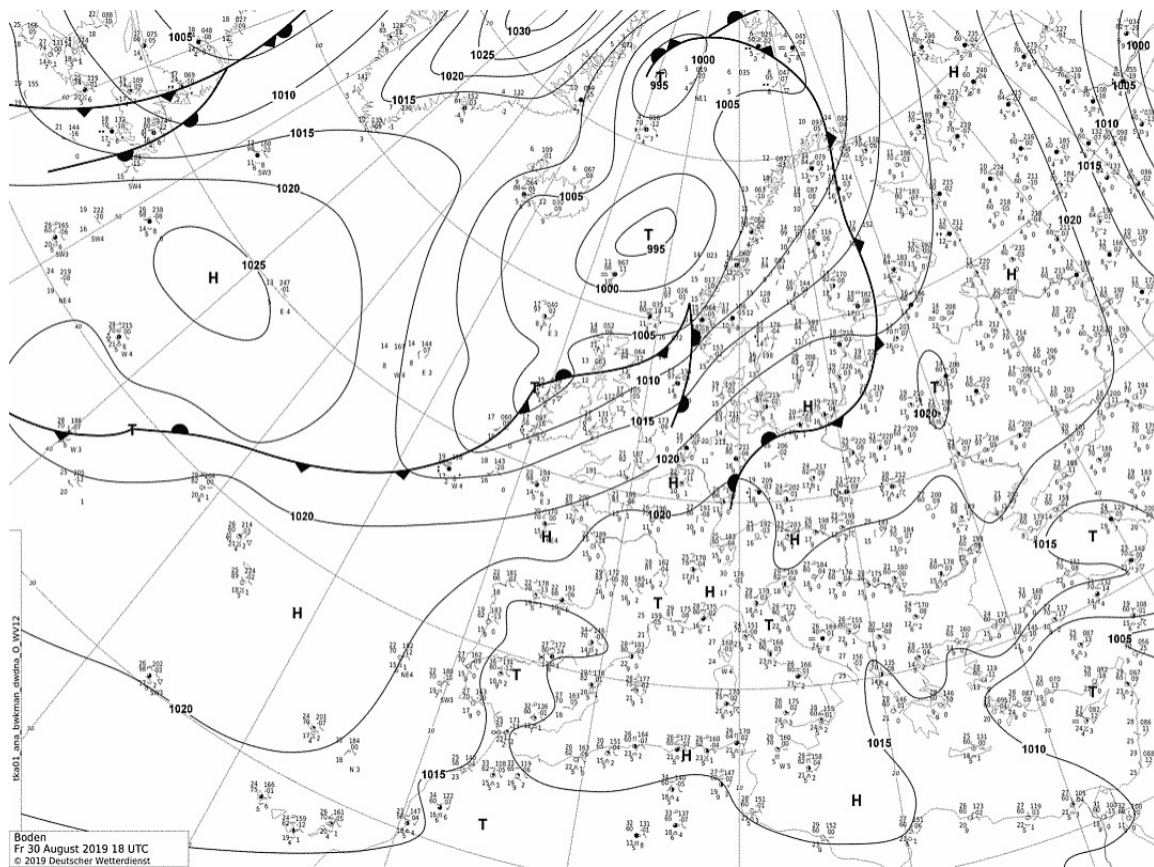


Figure 5.4: front analysis by DWD from 30.08.2019 at 18 UTC (<https://www.wetter3.de>)

Vaisala Radiosonde RS41-SGP

RS41 PTU Sensors

The Vaisala Radiosonde RS41 temperature sensor utilizes linear resistive platinum technology and is very stable. The small size of the sensor results in low solar radiation error and guarantees fast response. It also incorporates effective protection against evaporating cooling, a phenomenon occasionally encountered when a radiosonde emerges from a cloud top.

The humidity sensor integrates humidity and temperature sensing elements. Pre-flight automatic reconditioning of the humidity sensor effectively removes chemical contaminants and ensures excellent humidity measurement accuracy. The integrated temperature sensor is used to compensate the effects of solar radiation in real time. The sensor heating function enables an active and effective de-icing method at freezing conditions during the flight. The humidity sensor also responds quickly to detect fine structures of the atmosphere.

The pressure sensor is the same high-quality, shock-resistant capacitive silicon sensor as the one in the Vaisala Radiosonde RS92 with revised electronics and calibration.

All the RS41 sensors are calibrated against references that are traceable to international standards (SI units) and measurement uncertainties are estimated according to recommendations of the Joint Committee for Guides in Metrology, 100:2008.

Carrying Out Ground Checks on a RS41 Radiosonde

Radiosonde preparation involves several steps, including sensor functionality checks and setting the desired options for in-flight operational parameters, like timer to power off the radiosonde at the desired time, pressure, or altitude. During the preparation procedure the operator can also set the transmitter frequency of the radiosonde or apply the station default frequency.

The ground check device is conveniently operated with Vaisala MW41 software. A short-range wireless communication link is used for powering on the radiosonde and for data transfer during the ground check.

The in-built temperature sensor check includes a comparison of readings from the temperature element of the humidity sensor and the actual temperature sensor, although no correction to radiosonde measurement is applied.

With the new humidity sensor design, the radiosonde is able to generate physical zero humidity reference more consistently than is possible with desiccants. The sensor can measure the deviation of humidity measurement at physical zero (0 %RH) and fine-tune the humidity measurement accordingly.

For the pressure measurement ground check, the sounding software MW41 displays the RS41 pressure sensor reading difference against an optional barometer module installed inside the ground check device, and adjusts the measurement accordingly. Alternatively an external precision barometer can be used as the reference value and the readings entered manually.

Wind Data and GPS-Based Height and Pressure Measurements

Wind, as well as height and pressure readings are derived from velocity and location measurements of the RS41 GPS receiver. Wind is calculated independently based on satellite carrier frequency changes. With RS41-SGP height and pressure are also calculated from satellite ranging codes, combined with differential corrections from the MW41 ground station, as with RS41-SG.

Data Transmission

The Vaisala Radiosonde RS41 has a proven data transmission range from radiosonde to receiver of up to 350 km. Data availability during a sounding is guaranteed with digital error-correction code transmission, and telemetry errors are always detected. Due to narrower band transmission, more channels are available in the meteorological frequency band.

Operational Benefits

The RS41's robust and compact design makes it easy to handle and there is no assembly needed prior to launch. The status LED indicates when the radiosonde



Vaisala Radiosonde RS41-SGP – accuracy and reliability.

Benefits

- Superior PTU measurement performance with a pressure sensor
- Automated ground check
- Robust and easy-to-use
- GPS for continuous wind data availability as well as additional height and pressure calculation
- Stable narrow-band transmission complies with ETSI standard EN 302 054

is ready to launch, and if there is an error, it is clearly indicated prior to launch. With the unwinder the radiosonde sensor boom is automatically and consistently set in an ideal position for sounding.

Add-On Sensor Connector

The RS41 has an interface for additional sensors, primarily to connect it to the ozone interface OIF411. Other sensors with Xdata protocol can also be connected. The data is transferred either directly or via a OIF411 interface to a RS41 radiosonde and onward to the Vaisala DigiCORA® Sounding System MW41.

Technical Data

Measurements

Measurement cycle	1 s
TEMPERATURE SENSOR TYPE: PLATINUM RESISTOR	
Measurement range	+60 °C to -90 °C
Resolution	0.01 °C
Response time (63.2%, 6 m/s flow, 1000 hPa) ¹⁾	0.5 s
Stability (1 year / 3 years)	< 0.05 °C / < 0.1 °C
Accuracy (Repeatability & Combined uncertainty with k=2)	
Repeatability in calibration	0.1 °C
Combined uncertainty after ground preparation	0.2 °C
Combined uncertainty in sounding < 16 km	0.3 °C
Combined uncertainty in sounding > 16 km	0.4 °C
Reproducibility in sounding > 100 hPa ²⁾	0.15 °C
Reproducibility in sounding < 100 hPa ²⁾	0.30 °C
HUMIDITY SENSOR TYPE: THIN-FILM CAPACITOR	
Measurement range	0 to 100 %RH
Resolution	0.1 %RH
Response time	
6 m/s, 1000 hPa, +20 °C	< 0.3 s
6 m/s, 1000 hPa, -40 °C	< 10 s
Accuracy (Repeatability & Combined uncertainty with k=2)	
Repeatability in calibration	2 %RH
Combined uncertainty after ground preparation	3 %RH
Combined uncertainty in sounding	4 %RH
Reproducibility in sounding ²⁾	2 %RH
PRESSURE TYPE: SILICON CAPACITOR	
Measurement range	from surface pressure to 3 hPa
Resolution	0.01 hPa
Accuracy (Repeatability & Combined uncertainty with k=2)	
Repeatability in calibration	
> 100 hPa	0.4 hPa
100 - 3 hPa	0.3 hPa
Combined uncertainty in sounding	
> 100 hPa	1.0 hPa
100 - 3 hPa	0.6 hPa
Reproducibility in sounding ²⁾	
> 100 hPa	0.5 hPa
100 - 3 hPa	0.3 hPa
WIND SPEED	
Velocity measurement uncertainty ⁴⁾	0.15 m/s
Resolution	0.1 m/s
Maximum reported wind speed ³⁾	160 m/s
WIND DIRECTION	
Directional measurement uncertainty ⁴⁾	2 deg
Resolution	0.1 deg
Wind direction range	0 to 360 deg

Telemetry

Transmitter type	Synthesized
Frequency band	400.15 – 406 MHz
Tuning range	400.16 – 405.99 MHz
Maximum transmitting range	up to 350 km
Frequency stability, 90 % probability	± 2 kHz
Deviation, peak-to-peak	4.8 kHz
Emission bandwidth	According to EN 302 054
Output power (high-power mode)	min. 60 mW
Sideband radiation	According to EN 302 054
Modulation	GFSK
Data downlink	4800 bit/s
Frequency setting	Wireless with ground check device

GPS receiver (SA Off, PDOP<4)

Number of channels	≥ 48
Frequency	1575.42 MHz, L1 C/A code
Cold Start Acquisition Time	35 s (nominal)
Reacquisition Time	1 s (nominal)
Correction	Differential
Reporting resolution of lat, lon position values	1e-8°

Operational Data

Power-up	Wireless with ground check device or with switch
Factory calibration	Stored on Flash memory
Battery	2 pcs AA-size Lithium cells
Operating time	> 240 min
Weight EPS/plastic covers	84 g / 113 g
Dimensions ⁵⁾	Body (L x W x H): 155 x 63 x 46 mm
	Sensor boom bent (L x W x H): 282 x 63 x 104 mm

Add-On Sensor Support

Protocol support	Xdata to connect several sensors in the same chain, data transferred either directly or via OIF411 to RS41
Transfer rate	max. 200 bytes/s

Unwinder

Material of the string	Non-UV treated polypropylene
Tenacity	< 115 N
Length of the string	55 m
Unwinding speed	0.35 m/s
Weight	25 g

The performance data is expressed with 2-sigma confidence level (k=2), unless otherwise explicitly specified.
For humidity, the performance data is valid T > -60 °C.

- 1) After applying time-lag correction, the effect to measurement uncertainty is negligible.
- 2) Standard deviation of differences in twin soundings, ascent rate above 3 m/s for temperature and humidity
- 3) In practice unlimited
- 4) Standard deviation of differences in twin soundings. Wind speed above 3 m/s for directional measurement uncertainty.
- 5) For EPS cover; without wire antenna

VAISALA

Please contact us at
www.vaisala.com/requestinfo



Scan the code for more information

Ref. B211444EN-E ©Vaisala 2017

This material is subject to copyright protection, with all copyrights retained by Vaisala and its individual partners. All rights reserved. Any logos and/or product names are trademarks of Vaisala or its individual partners. The reproduction, transfer, distribution or storage of information contained in this brochure in any form without the prior written consent of Vaisala is strictly prohibited. All specifications – technical included – are subject to change without notice.

www.vaisala.com



Bibliography

- Baars, H., Radenz, M., Floutsi, A. A., Engelmann, R., Althausen, D., Heese, B., Ansmann, A., Flament, T., Dabas, A., Trapon, D., Reitebuch, O., Bley, S., and Wandinger, U. (2021). Californian wildfire smoke over europe: A first example of the aerosol observing capabilities of aeolus compared to ground-based lidar. *Geophysical Research Letters*, 48(8):e2020GL092194. e2020GL092194 2020GL092194.
- Butler, A. H., Sjoberg, J. P., Seidel, D. J., and Rosenlof, K. H. (2017). A sudden stratospheric warming compendium. *Earth System Science Data*, 9(1):63–76.
- NOAA (accessed 14.09.2022). Global data assimilation system (gdas). <https://catalog.data.gov/dataset/global-data-assimilation-system-gdas-3b35f>.
- NOAA (last updated 05.03.2021). Global data assimilation system (gdas1) archive information. <https://www.ready.noaa.gov/gdas1.php>.
- Pearson, K. (1905). "das fehlergesetz und seine verallgemeinerungen durch fechner und pearson." a rejoinder. *Biometrika*, 4(1/2):169.
- Schönwiese, C.-D. (2013). *Praktische Statistik für Meteorologen und Geowissenschaftler*. Borntraeger, Stuttgart, 5., vollst. überarb. und erw. aufl. edition. Mit 80 Abb., 66 Tabellen im Text und 11 Tabellen im Anhang. - Literaturverz. S. [295] - 302.
- Stahel, W. A. (2008). *Statistische Datenanalyse: eine Einführung für Naturwissenschaftler*. Studium. Vieweg, Wiesbaden, 5., überarb. aufl. edition.
- Tuononen, M., O'Connor, E. J., and Sinclair, V. A. (2019). Evaluating solar radiation forecast uncertainty. *Atmospheric Chemistry and Physics*, 19(3):1985–2000.
- Westfall, P. H. (2014). Kurtosis as peakedness, 1905–2014.r.i.p. *The American Statistician*, 68(3):191–195.

Statement of Authorship

I hereby certify that this bachelor thesis has been composed by myself and describes my own work, unless otherwise acknowledged in the text. All references have been quoted and all sources of information have been specifically acknowledged. It has not been accepted in any previous application for a degree.

Leipzig, 09.10.2022

A handwritten signature in black ink, appearing to read 'Baumer', with a long horizontal stroke extending to the right.

(Finja Baumer)